Tropospheric emission spectrometer for the Earth Observing System's Aura satellite

Reinhard Beer, Thomas A. Glavich, and David M. Rider

The Tropospheric Emission Spectrometer (TES) is an imaging infrared Fourier-transform spectrometer scheduled to be launched into polar Sun-synchronous orbit aboard the Earth Observing System's Aura satellite in June 2003. The primary objective of the TES is to make global three-dimensional measurements of tropospheric ozone and of the physical–chemical factors that control its formation, destruction, and distribution. Such an ambitious goal requires a highly sophisticated cryogenic instrument operating over a wide frequency range, which, in turn, demands state-of-the-art infrared detector arrays. In addition, the measurements require an instrument that can operate in both nadir and limb-sounding modes with a precision pointing system. The way in which these mission objectives flow down to the specific science and measurement requirements and in turn are implemented in the flight hardware are described. A brief overview of the data analysis approach is provided.

OCIS codes: 010.1280, 010.4950, 010.7030, 120.0280, 120.6200, 300.6300.

1. Introduction

A. Earth Observing System's Aura Satellite

In January 1988, NASA invited proposals for participation in a new program of polar Sun-synchronous orbiting platforms to be called the Earth Observing System (EOS). The objectives of this program have been stated in a variety of forms but most succinctly as a series of questions[1]:

(1) What are the nature and extent of land-cover and land-use change and the consequences for sustained productivity?

(2) How can we enable regionally useful forecasts of precipitation and temperature to be made in seasonal-to-interannual time frames?

(3) Can we learn to predict natural hazards and mitigate natural disasters?

(4) What are the causes and effects of long-term climate variability, and can we distinguish natural from human-induced drivers?

(5) How and why are concentrations and distributions of atmospheric ozone changing?

Use of the Tropospheric Emission Spectrometer (TES) was successfully proposed for this mission; the particular emphasis was on answering question (5) but with some useful applications for questions (2)–(4).

After a number of program reviews and restructurings, the spaceborne part of the program was divided into three parts: a largely Earth-surface-oriented platform called Terra; a second platform, named Aqua, to concentrate on climate; and a third one, called Aura, to study the chemistry of the troposphere and the lower stratosphere. The TES was assigned to the last-named platform, as were three other instruments: the Microwave Limb Sounder (MLS), the High Resolution Dynamics Limb Sounder (HiRDLS) and the Ozone Measuring Instrument (OMI). The Aura satellite (Fig. 1) will be launched in June 2003 into a Sun-synchronous orbit with a nominal 1:45 p.m. (local mean solar time) equator crossing. The orbit repeats exactly every 16 days (=233 orbits), with a near repeat every 2 days.

B. Troposphere

The troposphere is the region of the Earth's lower atmosphere that is dominated by convective processes. It extends from the surface of the Earth, with declining temperature, to the boundary with the stratosphere (the tropopause). The height of the

The authors are with the Jet Propulsion Laboratory, MS 183-301, California Institute of Technology, 4800 Oak Grove Drive, Pasadena, California 91109-8001. The e-mail address for R. Beer is reinhard.beer@jpl.nasa.gov.

Received 9 March 2000; revised manuscript received 26 January 2001.

0003-6935/01/152356-12$15.00/0

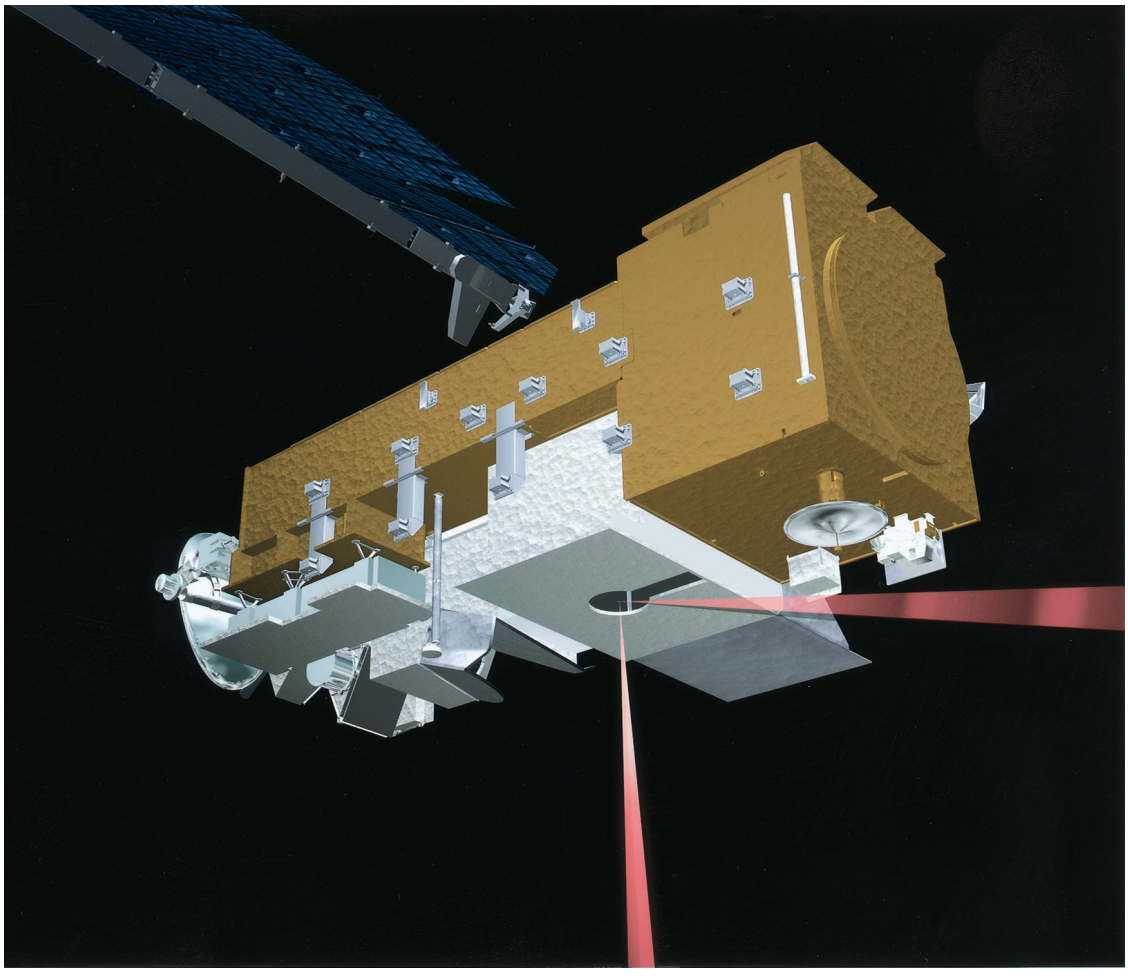

Fig. 1. Computer-aided design view of the EOS Aura platform on orbit. The TES is the instrument slightly to the right of center. The keyhole-shaped entrance aperture permits both downward and limb views to be obtained (indicated by the rays emanating from the aperture).

tropopause varies with latitude and season; it is generally highest in the tropics and lowest at the poles. An average thermal structure of the atmosphere is shown in Fig. 2.

The troposphere is, in turn, often subdivided into vertical zones. The lowest 1–2 km is termed the boundary layer, a region of strong horizontal and vertical mixing. Above this is the free troposphere, where much of the important photochemistry occurs. At the top is the upper troposphere, wherein transport to and from the stratosphere becomes important.

C. Specific Tasks of the TES

The primary task of the TES is to map the global three-dimensional distribution of tropospheric ozone and the chemical species involved in its formation and destruction (so-called precursors). Performing this task is an ambitious objective because only ~10% of the total ozone in the Earth's atmosphere is in the troposphere (most is in the stratosphere through which, of course, any spaceborne system must observe) and because many of the critical precursors exist only at very low concentrations (fractions of 1 part in 10^9 by volume). Therefore making the necessary measurements requires a carefully designed high-performance instrument. In particular, such low concentrations can generally be measured only by the technique of limb sounding (a sideways view through the atmosphere), which increases the path length some 100-fold at the expense of its suffering poorer spatial resolution along the line of sight. Furthermore, the penetration depth of limb sounders into the lower atmosphere is limited by the high probability of clouds in the line of sight, and even in cloud-free areas the ubiquitous water vapor continuum eventually becomes the limiting factor.

The major species, however, such as ozone, water vapor, carbon monoxide, and methane, have prominent spectral features even in nadir viewing (where the probability of seeing through gaps is much higher than in the limb but the vertical resolution is much poorer), so an initial requirement of the TES is that it provide both limb and nadir sounding capability. These two types of observation can be used in a synergistic mode so the resultant profiles can be concatenated, most effectively in a data assimilation process.

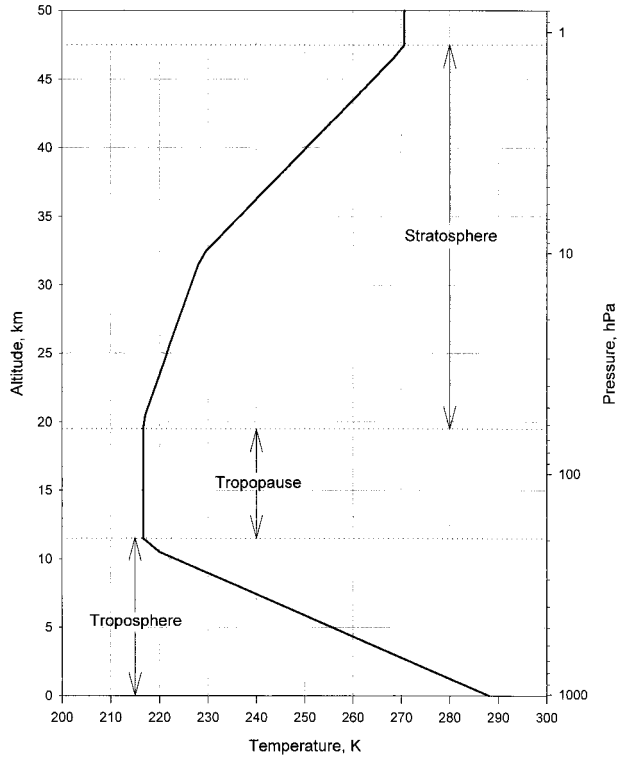

Fig. 2. 1976 U.S. Standard Atmosphere Temperature Profile showing the conventional names of the divisions of the vertical structure.

D. Tropospheric Ozone

Ozone is produced in the troposphere by photochemical oxidation of carbon monoxide and hydrocarbons in the presence of nitrogen oxides (NO_x) and water vapor. These ozone precursors have both natural and anthropogenic sources. The chemistry of ozone is complex and tightly coupled to the atmospheric transport of both ozone and its precursors. Tropospheric ozone affects the environment in three major ways:

(1) As an air pollutant. Ozone in surface air is toxic to humans, animals, and vegetation. It is the principal harmful component of smog.

(2) As a cleansing agent. Photolysis of ozone in the presence of water vapor is the primary source of the hydroxyl radical (OH), which is the main oxidant in the atmosphere. Reactions with OH in the lower and middle troposphere are the principal sink for a large number of environmentally important species, including air pollutants (CO), greenhouse gases (CH_4), and gases (hydrochlorofluorocarbons, methyl halides) that deplete the stratospheric ozone layer.

(3) As a greenhouse gas. Ozone in the middle and upper troposphere is an efficient greenhouse gas. Perturbation of ozone in this region of the atmosphere results in heterogeneous radiative forcing with complicated implications for climate.

The environmental implications of tropospheric ozone are therefore quite different from those of stratospheric ozone. The ozone layer in the stratosphere shields the Earth's surface from solar UV-*B* radiation, and thinning of this layer as a result of human activities is a matter of grave concern. Tropospheric ozone, by contrast, has increased as a consequence of human activity (primarily because of combustion processes). Whether this increase in tropospheric ozone is beneficial (cleansing agent) or harmful (air pollutant, greenhouse gas) depends to a large extent on its altitude. It is important, therefore, to map the global three-dimensional distribution of tropospheric ozone and its precursors to improve our understanding of the factors that control ozone in different regions of the troposphere.

Table 1. TES Standard Products and Required Sensitivity[a]

Product Name	Product Source: Nadir	Product Source: Limb	Required Sensitivity[b]
Level 1A interferograms	Yes	Yes	–
Level 1B spectral radiances	Yes	Yes	–
Atmospheric temperature profile	Yes	Yes	0.5 K
Surface skin temperature	Yes	No	0.5 K
Land surface emissivity[c]	Yes	No	0.01
Ozone (O_3) VMR profile	Yes	Yes	1–20 ppbv
Water vapor (H_2O) VMR profile	Yes	Yes	1–200 ppmv
Carbon monoxide (CO) VMR profile	Yes	Yes	3–6 ppbv
Methane (CH_4) VMR profile	Yes	Yes	14 ppbv
Nitric Oxide (NO) VMR profile	No	Yes	40–80 pptv
Nitrogen dioxide (NO_2) VMR profile	No	Yes	15–25 pptv
Nitric acid (HNO_3) VMR profile	No	Yes	1–10 pptv
Nitrous oxide (N_2O) VMR profile	Yes	Yes	Control[d]

[a]VMR, volume mixing ratio.
[b]Sensitivity range maps to expected concentration range (higher concentration means higher uncertainty): ppbv, parts in 10^9 by volume; ppmv, parts in 10^6 by volume: pptv, parts in 10^3 by volume. Some species (notably NO_x) will require some signal averaging to meet requirements.
[c]Water (and, probably, snow and ice) emissivities are known and are therefore input, not output, parameters.
[d]Tropospheric concentration known.

E. TES Data Products

In the EOS program, data products are divided into two classes: standard products, which are produced routinely and archived in a publicly accessible location, and special products, which have more of a research nature and are produced on an on-demand and noninterference basis.

The standard products that the TES will produce are global-scale vertical concentration profiles (0–~35 km) of ozone, water vapor, carbon monoxide, methane, nitric oxide, nitrogen dioxide, and nitric acid (the last two in the middle and the upper troposphere only) every other day for 5 years. Essential by-products of the analysis are atmospheric temperature profiles and surface temperature and emissivity. Table 1 lists the standard products, and Table 2 is a partial list of potential special products. In both cases, indications of the necessary observation conditions are included.

Table 2. Potential Special (Research) Products

Chemical Group	Common Name	Formula	Product Source: Nadir	Product Source: Limb
H_xO_y	Hydrogen peroxide	H_2O_2	No	Yes
	Monodeuterated water vapor	HDO	Yes	Yes
C compounds	Ethane	C_2H_6	No	Yes
	Acetylene	C_2H_2	No	Yes
	Formic acid	HCOOH	Yes	Yes
	Methyl alcohol	CH_3OH	Yes	Yes
	Peroxyacetyl nitrate	$CH_3C(O)OONO_2$	No	Yes
	Acetone	$CH_3C(O)CH_3$	No	Yes
	Ethylene	C_2H_4	No	Yes
N compounds	Peroxynitric acid	HO_2NO_2	No	Yes
	Ammonia	NH_3	Yes[a]	Yes
	Hydrogen cyanide	HCN	No	Yes
	Dinitrogen pentoxide	N_2O_5	No	Yes
Halogen compounds	Hydrogen chloride	HCl	Yes[a]	No
	Chlorine nitrate	$ClONO_2$	No	Yes
	Carbon tetrachloride	CCl_4	No	Yes
	CFC-11	CCl_3F	Yes	Yes
	CFC-12	CCl_2F_2	Yes	Yes
	HCFC-21	$CHCl_2F$	No	Yes
	HCFC-22	$CHClF_2$	No	Yes
S compounds	Sulfur dioxide	SO_2		Yes
	Carbonyl sulfide	OCS		Yes
	Hydrogen sulfide	H_2S	Yes[a]	Yes
	Sulfur hexafluoride	SF_6	No	Yes

[a]Volcanic–industrial–biomass burning plume column densities only.

2. Measurement Requirements and Approaches

The science requirements outlined above lead directly to a set of instrument and measurement requirements, listed in Table 3. The detailed bases and justification for these requirements are far too long to describe here, so only a brief outline follows. Further details can be made available on request.[2]

1. *Spectral Properties*

First, the species to be observed have their transitions widely scattered throughout the infrared, so an initial requirement is for broad spectral coverage (650–3050 cm^{-1}). Second, we want the spectral resolution to match the widths of the spectral features. Near the surface, weak Lorentz-broadened lines have a width of ~0.1 cm^{-1}, falling to ~0.025 cm^{-1} in the upper troposphere. Note that, within a factor of ~2, these widths are independent of species and frequency, so we have chosen those values for the nadir and limb spectral resolutions, respectively. In turn, maximum optical path differences of 8.45 cm in the nadir and 33.8 cm at the limb are required, resulting in spectral sampling distances of 0.0592 and 0.0148 cm^{-1}, respectively. For a number of reasons, it is preferable that the zero path difference be in the middle of the travel, so these values are bidirectional. For example, when one is using single-sided interferograms it is always necessary to overrun the zero path difference by as much as 10% to ensure that phase correction will work properly. Doing this is inefficient: Double-sided interferograms use the observation time more effectively (a vital property in a space experiment) and provide much more-robust phase correction.

2. *Scan Speed*

We have chosen to use a constant-speed mechanism to change the optical path difference to simplify the speed-control algorithm. This change results in scan times of 4 s in the nadir and 16 s at the limb.

3. *Spectrometer Type*

The foregoing requirements lead inevitably to a Fourier-transform spectrometer[3] (FTS) because dispersive spectrometers do not have constant (frequency) resolution and because gas-correlation spectrometers are limited in the kinds of species that they can observe and cannot cope with Doppler shifts, and other technologies offer only restricted spectral coverage. We have chosen the Connes-type four-port configuration[4] because (as we discuss below) it permits us to optimize detector technologies by using four relatively limited spectral regions that are further subdivided into 200–300-cm^{-1} bands through the use of interchangeable filters for background control and data-rate reduction.

4. *Detector Arrays*

One of the features of a FTS is that it readily supports an imaging mode, which, in turn, improves collection efficiency compared with those of the more traditional spatially scanning systems. We have chosen to employ 1 × 16 linear arrays, each of whose individual field of view is 0.75 × 7.5 mrad (Fig. 3). At

Table 3. TES Requirements and Specifications

Requirement	Specification	Comments
Spectrometer type	Connes-type four-port Fourier transform spectrometer	Both limb and nadir viewing capability essential
Spectral sampling distance	Interchangeably 0.0592 cm^{-1} downlooking and 0.0148 cm^{-1} at the limb	Unapodized
Optical path difference	Interchangeably ±8.45 cm downlooking and ±33.8 cm at the limb	Double-sided interferograms
Overall spectral coverage	650–3050 cm^{-1} (3.2–15.4 μm)	Continuous, but with multiple subranges typically 200–300 cm^{-1} wide (Table 4)
Individual detector array spectral coverage (cm^{-1})	1A, 1900–3050	All mercury cadmium telluride photo voltaic at 65 K. For the labeling convention see Fig. 3.
	1B, 820–150	
	2A, 1100–1950	
	2B, 650–900	
Detector array configuration	1 × 16	All four arrays optically conjugated
Aperture	5 cm	Unit magnification system
System étendue (per pixel)	9.45×10^{-5} cm^2 sr	Not allowing for a small central obscuration from the Cassegrain secondaries
Modulation index	>0.7; 650–3050 cm^{-1}	>0.5 at 1.06 μm (control laser)
Spectral accuracy	±0.000 25 cm^{-1}	After correction for finite field of view, off axis effects, Doppler shifts, etc.
Channeling	<10% peak to peak; <1% after calibration	All planar transmissive elements wedged
Spatial resolution	0.5 × 5 km nadir; 2.3 × 23 km limb	See Fig. 3
Spatial coverage	5.3 × 8.5 km nadir; 37 × 23 km limb	See Fig. 3
Pointing accuracy	75 μrad pitch, 750 μrad yaw, 1100 μrad roll	Peak-to-peak values
Field of regard	45° cone about nadir plus trailing limb	Also views internal calibration sources
Scan (integration) time	4-s nadir and calibration, 16-s limb	Constant-speed scan, 4.2 cm/sec (optical path difference rate)
Maximum stare time, nadir	208 s	40 downlooking scans
Transect coverage	885 km maximum	See Fig. 7
Interferogram dynamic range	≤16 bits	Plus four switchable gain steps
Radiometric accuracy	≤1 K, 650–2500 cm^{-1}; ≤2 K, 2500–3050 cm^{-1}	Internal, adjustable, hot blackbody + cold space
Pixel-to-pixel cross talk	<10%	Includes diffraction, aberrations, carrier diffusion, etc.
Spectral signal-to-noise ratio	As much as 600:1; 30:1 minimum requirement	Depends on spectral region and target. General goal is to be source photon shot-noise limited
Lifetime	5 years on orbit	Plus 2 years before launch
Size	1.0 m × 1.3 m × 1.4 m	Earth shade stowed
Mass	385 kg	Allocation
Power, average	334 W	Allocation
Power, peak	361 W	Allocation
Data rate, average	4.5 MBPS	Science only
Data rate, peak	6.2 MBPS	Allocation

the trailing limb, some 3100 km distant, these values translate to spatial resolutions of 2.3 km vertically and 23 km horizontally. Inasmuch as the same arrays are used in nadir (705-km range), the projections become 0.5 km in track and 5 km cross track at the Earth's surface.

The data from a FTS are highly sensitive to nonlinearities, so the decision was made to avoid using photoconductive detectors, which are well known to be inherently nonlinear. Thus all four arrays are made from photovoltaic mercury cadmium telluride. At the longer wavelengths, avoiding the use of photoconductive detectors has required a significant, but successful, technology development.

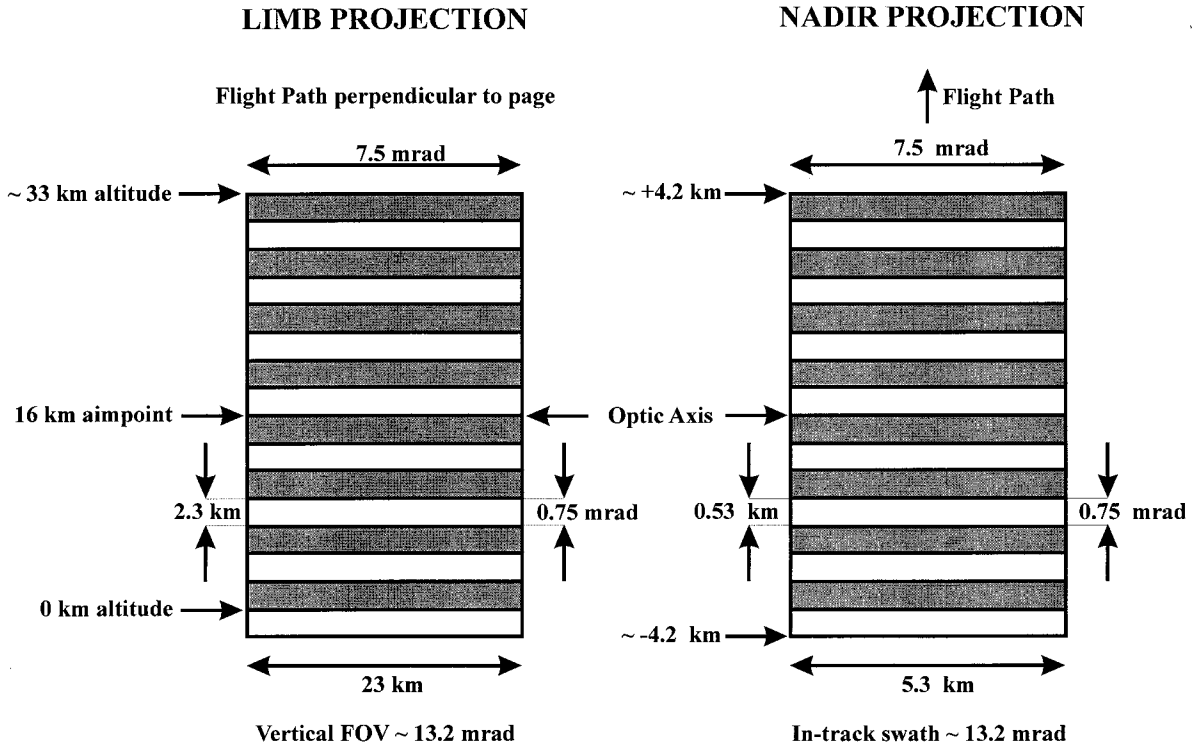

Fig. 3. TES detectors projected to the nadir (705-km range) and to the limb (3100-km range). Although they are shown as discrete elements, the pixels are, in fact, continuous but are defined by an array of contacts underneath. FOV, field of view.

5. Signal-to-Noise Ratio

It is readily demonstrated that, despite the generally higher signals, nadir retrievals are more demanding than limb retrievals because of the strong coupling between height resolution and precision. Doubling the number of nadir retrieval levels more than doubles the error. Furthermore, the inherent precision of limb retrievals is generally a factor of ~5 better than nadir retrievals because the height resolution of limb retrievals is determined by the viewing geometry, not by the physics of radiative transfer; the path length through the atmosphere is ~100 times greater than in nadir, thereby improving the detectability of trace species; and the background for limb observations is cold space, which provides improved spectral contrast. To retrieve ozone in the nadir with ~0.5 scale height resolution, we determined, through detailed simulations, that to meet the precision requirements of Table 1 requires a signal-to-noise ratio of at least 600:1 at 1050 cm^{-1}.[5] For all other species and temperatures, ratios of from 100:1 to 200:1 suffice. With a 5-cm aperture and a scan time of 4 s (nadir) or 16 s (limb), we found (using a radiometric model) that we should be able to meet or exceed these requirements under most conditions. However, for ozone itself, some pixel averaging will be necessary, and at frequencies above 2500 cm^{-1} limb sounding becomes impracticable.

6. Pointing Accuracy

We use the TES in a so-called staring mode to avoid amplitude modulations caused by scene variations (which can easily become the dominant noise source in a FTS). This, in turn, puts stringent requirements on the pointing accuracy. Unfortunately, using active feedback control from the scene (especially at the limb) is impracticable, so we must control the pointing mirror by dead reckoning, using gyro attitude signals from the spacecraft. The most difficult direction to measure is the pitch axis (the vertical direction at the limb), for which a specification of 75 μrad peak to peak is necessary owing to the extreme radiance gradients (as much as 40%/km) observed in the upper troposphere.

7. Field of Regard

The two-axis pointing mirror not only must stabilize the line of sight but must also permit switching the field of view from nadir to the (trailing) limb, to cold space above the limb, and to the internal calibration sources. The added benefit is that the TES is not limited to strictly nadir viewing: We can offset the downward view by as much as 45° in any direction and either stare at a location (a volcano, for example) for more than 3 min or, along the ground track, place the footprints contiguously to make transect observations that cover more than 800 km. This mode is valuable for observing phenomena such as the regional ozone episodes that invade the eastern United States in the summer.

3. Instrument Overview

A. Optical Layout

As indicated in Table 3 the TES is a Connes-type four-port imaging infrared FTS. Figure 4 is a sche-

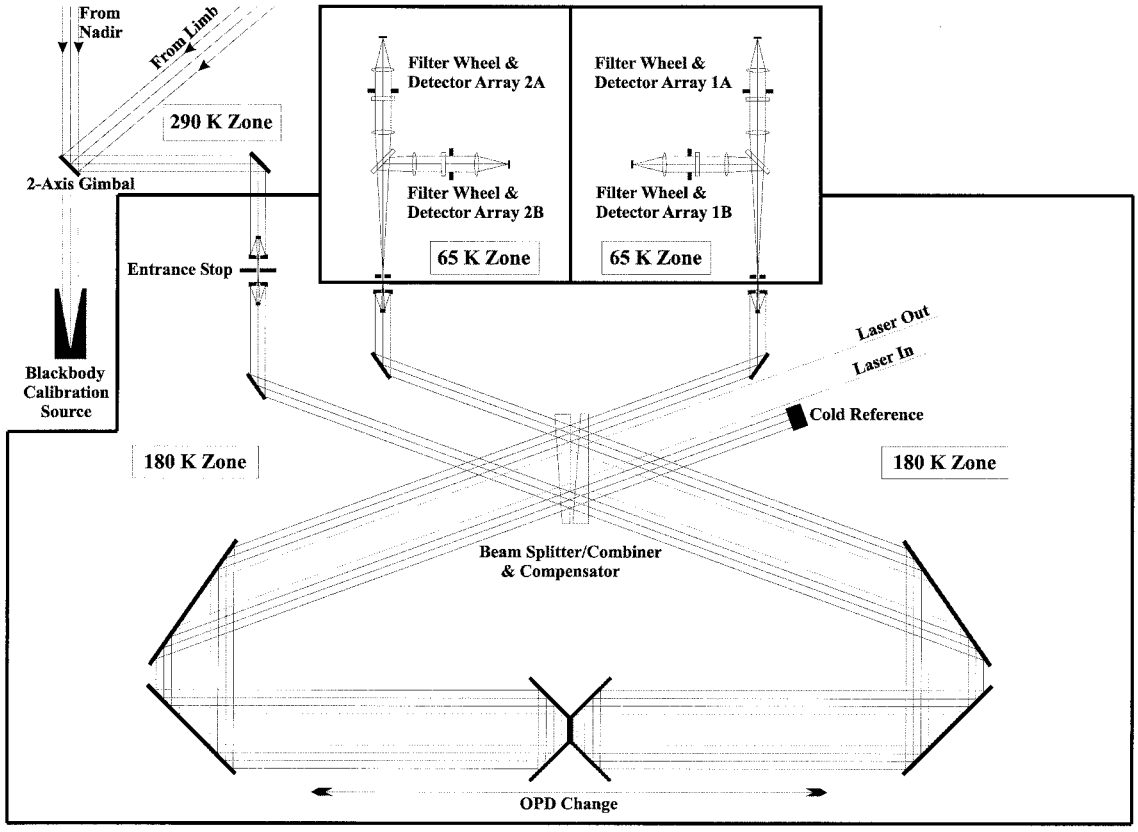

Fig. 4. TES optical schematic (Earth upward in this view). Light enters at the upper left. Note the three different temperature zones and the labeling of the four detector arrays.

matic of the optical path. Key features of the TES are the use of

(1) Back-to-back cube-corner reflectors on a common translator mechanism to provide the change in optical path difference.

(2) Potassium bromide (KBr) for the beam splitter–recombiner and the compensator. Whereas KBr has many desirable properties such as good infrared transmittance and a low refractive index, it has numerous less-desirable ones such as low strength and poor resistance to deformation and is, of course, hygroscopic. Although these properties certainly complicate handling and mounting, KBr has been used in space successfully in other instruments [e.g., the Atmospheric Trace Molecule Spectroscopy (ATMOS) spectrometer[6]].

(3) Only one of the two input ports for actual atmospheric measurements. The other input views an internal, grooved, cold reference target.

(4) A diode-pumped solid-state Nd:YAG laser for interferogram sampling control. The superior ruggedness, lower voltages and power dissipation of the Nd:YAG laser compared with those of a He–Ne laser, for example, make the Nd:YAG laser in our view, a better choice for a space platform despite the need for temperature control of the laser head.

(5) Cassegrain telescopes for condensing and collimating wherever possible to minimize the number of transmissive elements in the system. In the infrared, reflectances of 0.98–0.99 are routinely available, whereas, even with the best available antireflection coatings, the transmittances of space-qualified infrared transmitting materials (e.g., ZnSe) rarely exceed 0.95.

(6) A passive space-viewing radiator (see below) to maintain the interferometer and most of the associated optics at 180 K. This instrument reduces the thermal background noise and improves contrast between the scene and the instrument background.

(7) A two-axis gimbaled pointing mirror operating at ambient temperature to permit observation over the full field of regard (a 45° cone about nadir plus the trailing limb). Pointing is performed by dead reckoning: The gimbal axes have 21-bit shaft encoders attached, and, using these and spacecraft ephemeris and attitude information, the onboard computer calculates the necessary pointing angles.

(8) Two independent focal plane assemblies maintained at 65 K with active pulse-tube coolers. The assemblies accept the dual outputs of the interferometer (labeled as arrays 1A, 1B, 2A, and 2B in Fig. 4), which are further split by dichroics into A and B channels, hence the designations in Table 3. Thus there are four independent focal planes, each an array of 1×16 elements and optically conjugated such that equivalent pixels in each focal plane see the same target. Each focal plane is photovoltaic mer-

Table 4. Filter Bands and Species Coverage[a]

Filter Identification	Filter Half-Power Points (cm^{-1})		Temperature	Major Species
Array 2B (650–900 cm^{-1})				
2B1	650	900	T_a	CO_2, HNO_3, CFC11, NO_2
Array 1B (820–1150 cm^{-1})				
1B1	820	1050	T_b	HNO_3, NH_3, CFC11, CFC12, O_3
1B2	950	1150	T_b	O_3, NH_3, CFC11, CFC12, N_2O
Array 2A (1100–1950 cm^{-1})				
2A1	1100	1325	T_b	O_3, N_2O, HNO_3, CFC12, SO_2, CH_4
2A2	1300	1550		O_3, HNO_3, CH_4
2A3	1500	1750		H_2O, NO_2
2A4	1700	1950		H_2O, NO
Array 1A (1900–3050 cm^{-1})				
1A1	1900	2250	T_b	O_3, CO, N_2O, NO, OCS
1A2	2200	2450	T_a	CO_2, N_2
1A3	2425	2650	T_b	N_2O
1A4	2600	2850	T_b	HDO
1A5	2800	3050	T_b	CH_4, HCl, O_3

[a] T_a, atmospheric temperature profile; T_b, surface temperature and emissivity. CFC11, CCl_3F; CFC12, CCl_2F_2.

cury cadmium telluride optimized for a different spectral range (Table 3). In addition, each has an independent filter wheel in which the filters are typically 200–300 cm^{-1} wide (Table 4). These components not only reduce instrument background control but permit sampling of the interferograms in an upper alias[3] (the sampling interval is 8–11 laser fringes per sample) with a consequent reduction in data rate and volume (i.e., provide a form of lossless data compression).

B. Signal Chains

Each of the 16 pixels in each array has an independent signal chain (i.e., 64 in all). The implementation uses application-specific integrated circuits with four levels of switchable gain and switchable electronic bandpass filters (designed to match the optical band passes) for noise control. The gains are set at the beginning of each scan to a value determined by the expected signal at zero path difference (e.g., to the highest value for a space-view calibration and, conversely, to the lowest gain for observation of the onboard blackbody calibration source). The gains are not changed during the course of a scan because the signal chains have been designed to accommodate the full dynamic range of the signals without gain switching. Output is provided by 16-bit analog-to-digital converters triggered by the Nd:YAG laser subsystem. The digital outputs are multiplexed into a serial bit stream contained in a single packet and transmitted to the spacecraft by way of a TAXI interface. The output science data rate averages 4.5 megabits per second (MBPS).

C. Thermal and Mechanical

The instrument is contained in a box-shaped panel-and-web structure, largely of graphite–cyanate ester composites. The dimensions are 1.0 m × 1.3 m × 1.4 m. The nadir-viewing face serves as a radiator to reject heat from the electronics. Two radiating surfaces are mounted on the spaceviewing side of the instrument: One serves to cool a thermal shield surrounding the interferometer to 230 K and the other cools the interferometer to 180 K to minimize instrument self-emission. A deployable Earth shade protects these two radiating surfaces from earthshine.

Many of the heat-generating electronic subassemblies are mounted on the spacecraft side of the instrument for structural integrity, far from the nadir radiator. Propylene loop heat pipes,[7,8] in a technology that has only recently become available, are used to transport heat from these electronic assemblies to the nadir radiator. The advantages of loop heat pipes compared with more conventional heat pipes are that the efficiency of the former is largely independent of orientation or gravity and that they can be turned on and off at will. The ability to turn the loop heat pipes off is particularly important for instrument decontamination, for which it is imperative that heat losses from the instrument be minimized to conserve decontamination power.

The interferometer is built around a separate structure called an optics bench that is mounted in the interior of the main structure. The optics bench is also fabricated from graphite–cyanate ester composites, which are designed for a near-zero coefficient of thermal expansion along critical directions. The optics bench temperature is controlled with small heaters to minimize mechanical distortions caused by changing thermal gradients.

D. In-Flight Calibration

An emission-mode sensor such as a TES is critically dependent on accurate radiometric calibration if valid retrievals are to be made from its spectra. Accordingly, the TES has an internal full-aperture cavity blackbody source (identical to that used on the Measurements of Pollution in the Troposphere (MOPITT) instrument on the Terra spacecraft) to which the pointing mirror can be directed. The tempera-

ture of this blackbody is adjustable from ambient (~290 K) to 340 K. Most routine calibrations are performed at 340 K for the hot point and the cold space for the baseline (offset). Although photovoltaic detectors are much less susceptible to nonlinearity than photoconductive detectors, the potential for nonlinearity elsewhere in the signal chain always exists, so, from time to time, the internal source varies in temperature over its entire range so the effect (if any) can be monitored.

Most standard calibrations will be obtained at 0.0592-cm^{-1} spectral sampling distance and FFT interpolated for the limb scans at a 0.0148-cm^{-1} spectral sampling distance, it is presupposed that there are no sources of sharp-line spectral features internal to the TES. Occasionally, therefore, we shall acquire calibration data at the higher resolution to check this hypothesis.

The TES also has an onboard spatial calibrator (an illuminated slit) that the pointing mirror will sweep over the detector arrays to check the coalignment of the arrays.

E. Contamination

The TES is a cryogenic instrument and, as such, is highly susceptible to contamination from outgassing not only internally but also from the rest of the spacecraft. Most vulnerable, of course, are the focal planes (the coldest points in the system). We shall monitor this contamination through the calibration signals: When these signals fall by 5%, decontamination heaters will be turned on to raise the entire instrument temperature to ~285 K to drive off any condensates (which are expected to be primarily water vapor, carbon dioxide, and residual hydrocarbons).

4. Operational Modes

A. Introduction

As indicated above, the TES inherently operates in a step-and-stare mode when it is downlooking. At the limb the instrument points to a constant tangent height. The footprint is therefore smeared along the line of sight by ~110 km during a 16-s limb scan (comparable with the effective size of the footprint itself). Thus horizontal inhomogeneity in the atmosphere becomes an issue that must be dealt with in data processing (usually through a simplified form of tomography). Furthermore, the long path through the limb makes cloud interference almost inevitable; rarely does a limb view penetrate to the boundary layer. Nevertheless, the benefits of limb viewing for trace-gas analysis in the middle and upper troposphere are so great as to outweigh any disadvantages.

B. Global Surveys

The routine operating procedure for the TES is to make continual sets of nadir and limb observations (plus calibrations) on a 1-day-on, 1-day-off cycle. During the off days, extensive calibrations and special product observations are made (see below). The main argument for using such discontinuous sequencing is the sheer volume of data generated during each on day (~325 Gbytes). Such a volume stresses not only the data analysis process but, equally importantly, the ability of the scientific community to assimilate the information.

An overview of the acquisition process is shown in the upper part of Fig. 5. The lower part shows how this process is divided into 81.2-s sequences of calibration, nadir, and limb observations. The timing is based on the need for the sampling density to be commensurate with the approximately 5° latitude grid of current chemical–dynamic atmospheric models. Furthermore, acquisition is triggered by the crossing of the southernmost point in the orbit (the southern apex). Thus observations are made at the same latitudes during every orbit, and on every 16th day identical locations are sampled (Fig. 6).

C. Intensive Campaigns

Intensive campaigns fall under the special product rubric and are necessarily conducted in track. There are two types of campaign that are envisaged: downlooking transects and continuous limb observations. Transects involve pointing forward 45° and staring for one or more 4-s scans. The footprint is then stepped backward such that the new footprint is contiguous to the previous one (Fig. 7). Of course, the spacecraft is moving forward during this time at ~7 km/s, so eventually the transect passes through nadir and is terminated when the nadir angle is 45° backward. The 45° limit is somewhat arbitrary but is approximately the condition beyond which line-of-sight inhomogeneity and refraction would complicate the analysis. Furthermore, the footprint stretches as one goes off nadir, with a consequent loss of spatial resolution. Transects can be as much as 885 km long and will typically be used to study regional ozone episodes such as occur over the eastern United States in summer. Limb campaigns are unlimited in length and will usually be used to investigate phenomena such as effects on the upper troposphere of large volcanoes (exemplified by the Mt. Pinatubo eruption in 1991). Similar campaigns will be undertaken for intercomparisons with the other Aura instruments and in validation programs.

D. Special Events

Special events use the ability of the TES to point at specific locations for a few minutes on any given orbit. Notable among these targets are gas-emitting volcanoes (e.g., Mount Kilauea in Hawaii) whose gas admixtures are believed to be eruption predictors. Inasmuch as the TES can point anywhere within 45° of nadir (cross track and in track), almost every place on Earth can be reached sometime during a 16-day interval.

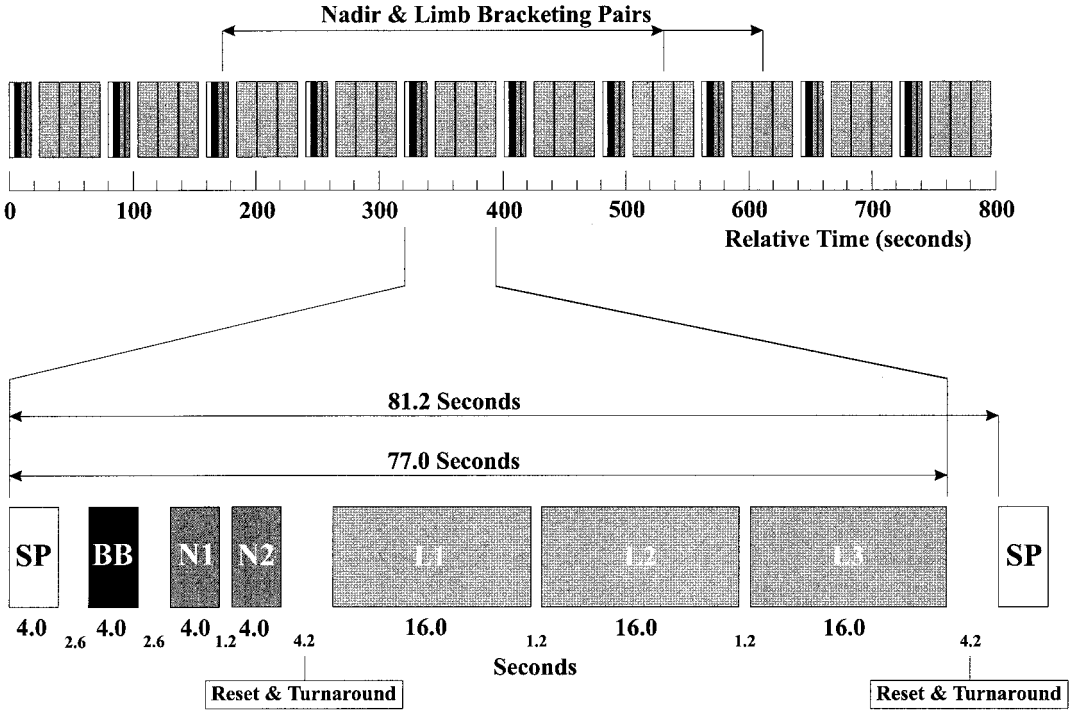

Fig. 5. Phasing of nadir and limb sequences: SP, 4-s space view calibration (~300-km altitude above the surface); BB, 4-s view of the internal 340-K blackbody; N1, N2, two 4-s atmosphere–surface scans of the same location near nadir, L1–L3, are three 16-s scans of the atmosphere at the trailing limb.

5. Data Analysis

TES data processing falls naturally into four groups (the "level" terminology is NASA's):

At Level 1A the raw data from the spacecraft are decommutated and the interferograms reconstructed. File headers also contain important ancillary data such as time, date, spacecraft and target location, and instrument pointing angle.

At Level 1B the interferograms are phase corrected and converted into spectra, radiometrically calibrated,

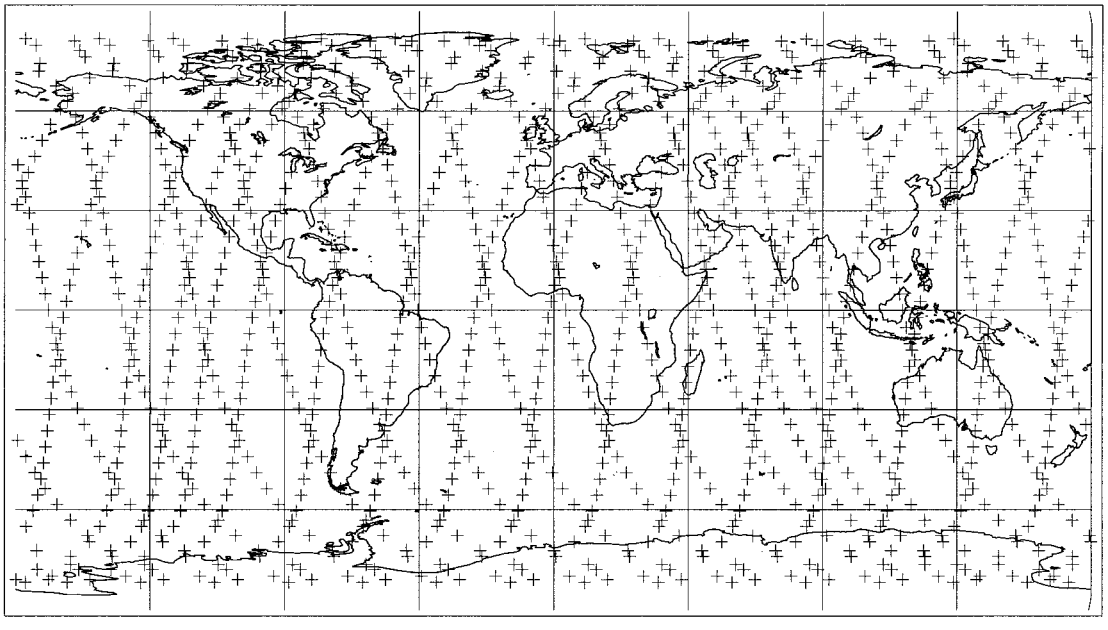

Fig. 6. Coverage during a typical day of a TES global survey (crosses). The Aura platform will be in a 705-km Sun-synchronous polar orbit with an exact 16-day repeat cycle. However, there is also a near-repeat every 2 days, so the mission plan of observing on alternate days ensures that these marked areas will be sampled repeatedly because the observation timing is designed to place TES footprints at the same latitudes on every orbit.

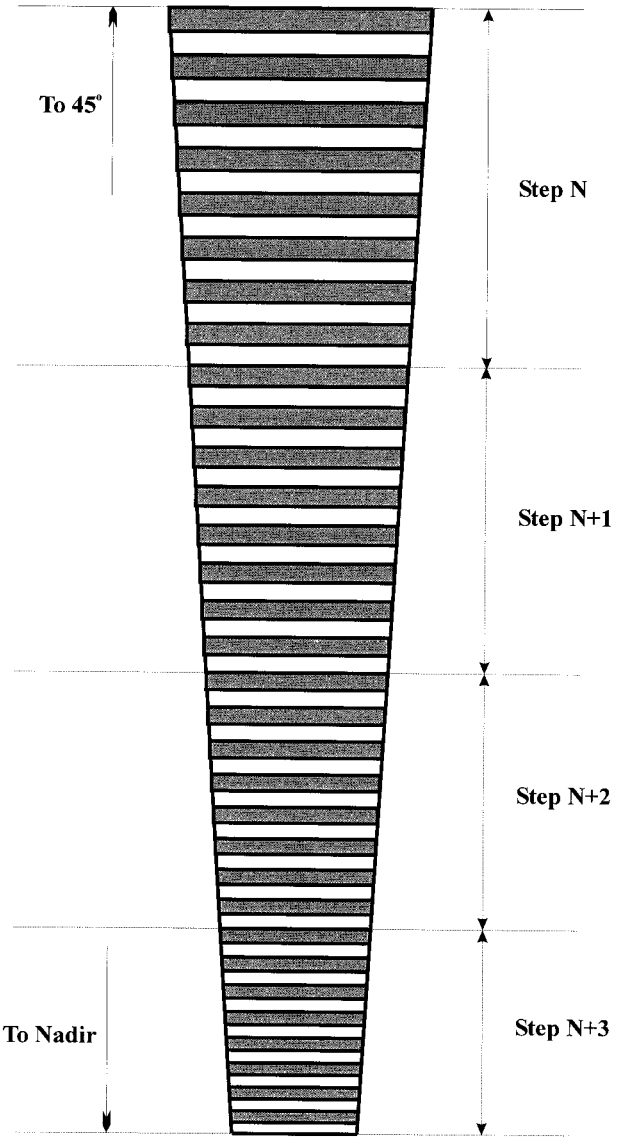

Fig. 7. Schematic of the TES transect mode. Beginning by pointing 45° forward (along track), successive footprints are laid end to end over a distance of as much as 885 km. The transect ends at a nadir angle of −45°. Note that the along-track expansion of the footprint (keystoning) is exaggerated for clarity.

corrected for off-axis instrument line-shape distortion,[9] and resampled onto a common frequency grid. Certain data quality flags are added to the header at this juncture, and the results passed to level 2. The algorithms are discussed in detail in Ref. 10.

At Level 2 vertical concentration profiles of the selected species are extracted from the spectra by use of a forward model based on a physical–chemical model of the expected atmospheric state followed by a retrieval with appropriately constrained optimal estimation techniques.[11] Accompanying the profiles are complete error covariance matrices to provide an objective estimate of the quality of the retrievals. Both the forward model and retrieval algorithms are discussed in detail in Ref. 12.

At Level 3 the profiles are resampled onto appropriate surfaces (usually pressure) to provide a series of maps (one set for each species). This, we believe, will be the most commonly used TES browse product, although serious users will then most likely request the level 2 profiles themselves.

Note that, by policy for the EOS data, all products are in the public domain and available from the archives at the marginal cost of reproduction. The TES data will be archived and available from the NASA Langley Research Center Distributed Active Archive Center in Hampton, Va.

6. Instrument Status

The design of the TES instrument has been complete and stable for several years. An engineering model of the interferometer was completed in 1999 and was found to provide a modulation index (one of the most critical parameters for a FTS) of 0.8, which is well above the requirement of 0.7. We are therefore confident that the flight instrument will perform to expectations on orbit.

As of December 2000, flight instrument assembly and testing have been in progress. This is a relatively slow process because the TES is a cryogenic instrument and can be tested only under thermal vacuum conditions (shrinkage between room temperature and the operating temperature of 180 K is significant), but, of course, the actual assembly occurs at room temperature. A sophisticated metrology system has therefore been devised to measure the changes with temperature such that appropriate mechanical offsets can be incorporated into the optical train.

Full flight calibration will begin in September 2001, and the TES is due to be delivered to the Aura spacecraft in April 2002.

7. Conclusions

Although inclusion of such information is uncommon in this type of paper, we believe that it is important that the reader be able to understand why specific instrument parameters and characteristics were chosen, flowing from the overall mission requirements down to the specific hardware implementation. In many cases, there were equally good or bad alternatives, but overriding requirements for any space experiment are cost and schedule. Reliability through redundancy is also preferred, but cost considerations have dictated that the TES be largely a single-string instrument with little or no duplication of parts.

We intend to discuss in a subsequent paper the measured characteristics of the TES compared with those of the preflight performance models on which much of the design is based. However, we have high confidence that the performance goals will be met because the TES shares many of the characteristics of an airborne precursor called the Airborne Emission Spectrometer (AES). The AES has flown many times on a variety of aircraft (a severe environment for any instrument) with good success[13,14] and has proved to be an invaluable test-bed both for hardware and for data analysis.

We should be remiss were we not to express our sincere thanks to the many individuals who have contributed to this program. The full list would run to well over 100 names, but we do especially wish to thank Robert J. McNeal of NASA headquarters for his longstanding support; Daniel Jacob and Jennifer Logan of Harvard University for keeping us focused on our primary objective; Tony Clough of AER, Inc., and Clive Rodgers of Oxford University for their keen analytical insights; and Edward Miller and Helen Worden of the Jet Propulsion Laboratory, without whom this instrument could never have been built.

The research reported in this paper was conducted by the Jet Propulsion Laboratory, California Institute of Technology, under a contract with the National Aeronautics and Space Administration.

References

1. "Earth Science Strategic Enterprise Plan 1998–2002" [NASA, Washington, D.C., 1998 (http://www.earth.nasa.gov/visions/stratplan/index.html)].
2. "Tropospheric Emission Spectrometer scientific objectives & approach, goals & requirements," V. 6.0, Rep. JPL D-11294 (Jet Propulsion Laboratory, Pasadena, Calif., 1999).
3. R. Beer, *Remote Sensing by Fourier Transform Spectrometry* (Wiley, New York, 1992).
4. J. Connes and P. Connes, "Near-infrared planetary spectra by Fourier spectroscopy. I Instruments and results," J. Opt. Soc. Am. **56,** 896–910 (1966).
5. S. A. Clough, C. P. Rinsland, and P. D. Brown, "Retrieval of tropospheric ozone from simulations of nadir spectral radiances as observed from space," J. Geophys. Res. **100,** 16579–16593 (1995).
6. C. B. Farmer, "High resolution infrared spectroscopy of the Sun and the Earth's atmosphere from space," Mikrochim. Ac **3,** 189–214 (1987).
7. D. A. Wolf, D. M. Ernst, and A. L. Phillips, "Loop heat pipes—their performance and potential," in *1994 SAE International Conference on Environmental Systems, Friedrichshafen, Germany, 20–23 June 1994* Society of Automotive Engineers, Warrendale, Pa. 15096), paper 941575.
8. M. Nikitkin, B. Cullimore, and J. Baumann, "CPL and LHP technologies: what are the differences, what are the similarities?" presented at the 9th Annual Spacecraft Thermal Control Technology Workshop Los Angeles, Calif., 4–6 March 1998.
9. K. W. Bowman, H. M. Worden, and R. Beer, "Instrument lineshape modeling and correction for off-axis detectors in Fourier-transform spectrometry," Appl. Opt. **39,** 3765–3773 (2000).
10. Jet Propulsion Laboratory, "Level 1B algorithm theoretical basis document," Rep. JPL D-16479 [Jet Propulsion Laboratory, Pasadena, Calif., 1999 (http:/www.eospso.gsfc.nasa.gov/atbd/pg1.html)].
11. C. D. Rodgers, *Inverse Methods in Atmospheric Sounding: Theory and Practice* (World Scientific, Singapore, 2000).
12. Jet Propulsion Laboratory, "Level 2 Algorithm Theoretical Basis Document," Rep. JPL D-16474 [Jet Propulsion Laboratory, Pasadena, Calif., 1999) (http:/www.eospso.gsfc.nasa.gov/atbd/pg1.html)].
13. H. M. Worden, R. Beer, and C. P. Rinsland, "Airborne infrared spectroscopy of 1994 western wildfires," J. Geophys. Res. **102,** 1287–1299 (1997).
14. V. J. Realmuto and H. M. Worden, "Impact of atmospheric water vapor on the thermal infrared remote sensing of volcanic sulfur dioxide emissions: a case study from the Pu'u O'o vent of Kilauea Volcano, Hawaii," J. Geophys. Res. **105,** 21,497–21,507 (2000).